Ceramics International 49 (2023) 20756–20762

Contents lists available at ScienceDirect

Ceramics International

journal homepage: www.elsevier.com/locate/ceramint

Thickness-dependent microstructure, resistive switching, ferroelectric, and energy storage properties of pulsed laser deposited 0.85[0.6Ba($Zr_{0.2}Ti_{0.8}$)O_3-0.4($Ba_{0.7}Ca_{0.3}$)TiO_3]-0.15$SrTiO_3$ thin films

Muhassinah Tasneem [a,1], Carlos R.P. Monteiro [b,c,1], N.S. Kiran Kumar [d], J.P.B. Silva [b,c,*], K.C. Sekhar [d], K. Kamakshi [a,**], M. Pereira [b,c]

[a] Department of Science and Humanities, Indian Institute of Information Technology Tiruchirappalli, Tiruchirappalli, 620 015, Tamil Nadu, India
[b] Centre of Physics of University of Minho and Porto (CF-UM-UP), Campus de Gualtar, 4710-057, Braga, Portugal
[c] Laboratory of Physics for Materials and Emergent Technologies, LapMET, University of Minho, 4710-057, Braga, Portugal
[d] Department of Physics, School of Basic and Applied Sciences, Central University of Tamil Nadu, Thiruvarur, 610 005, India

ARTICLE INFO

Handling Editor: Dr P. Vincenzini

Keywords:
BZCT-STO thin Films
Interface layer
Size effect
Ferroelectric
Resistive switching
Energy storage performance

ABSTRACT

In this work, we have studied the effect of thickness on structural, morphological, resistive switching (RS), ferroelectric, and energy storage properties of 0.85[0.6Ba ($Zr_{0.2}Ti_{0.8}$)O_3-0.4($Ba_{0.7}Ca_{0.3}$)TiO_3]-0.15$SrTiO_3$ (BZCT-STO) thin films deposited by the pulsed laser deposition technique. X-ray diffraction (XRD) analysis suggests that BZCT-STO thin films exhibit a polycrystalline tetragonal structure. The lattice parameters and tetragonality ratio approaching to bulk value with an increase of thickness, confirm strain relaxation in thicker films. SEM analysis reveals a dense columnar structure with a different grain size that varies from 3 nm to 60 nm as thickness increased from 160 to 360 nm. The P-E loops suggest that the relaxor behaviour increases with a decrease of thickness due to interface low dielectric layer, substrate clamping effect, small grain size, and high back switching ratio. The RS effect observed in Pt/BZCT-STO/Au capacitors is attributed to polarization modulation of the Schottky barrier and is found to be significant at low thickness. The effect of electric field and frequency on energy storage properties of BZCT-STO films is also investigated. The Pt/BZCT-STO/Au capacitor with a thickness of 160 nm exhibited 6.0 J/cm^3 with an efficiency of 72% at a field of 800 kV/cm. It also exhibited a robust energy storage performance in the frequency range of 50–2000 Hz and also up to 10^8 cycles passing through the capacitor.

1. Introduction

The potentiality of utilizing perovskite-based ferroelectric ceramics and thin films has been tremendously increasing in different applications including pulsed power systems, random access memories, and high-power microwave electronic systems due to their superior dielectric and ferroelectric characteristics like switchable polarization, low dielectric loss, spontaneity, high dielectric breakdown strength and nonlinear polarization-electric field (P-E) dependency [1–3]. Over the few decades, lead-based ceramics like lead lanthanum zirconate titanate (PLZT), lead magnesium niobate–lead titanate (PMN-PT) and lead zirconate titanate Pb(Zr,Ti)O_3 (PZT) compounds have been occupying the market because of their aforementioned properties and their outstanding performance in energy storage [4–7]. But due to their toxic nature and harmful effects on the human body and environment, researchers turned towards lead-free ferroelectric materials which include $BiFeO_3$ (BFO), $BaTiO_3$ (BTO), $K_{0.5}Bi_{0.5}TiO_3$ (KBT), ($Na_{0.5}K_{0.5}$)NbO_3 (NKN), (1−x)Ba($Zr_{0.2}Ti_{0.8}$)O_3–x($Ba_{0.7}Ca_{0.3}$)TiO_3 (BZCT) and modified BZCT ceramics [3,8].

In this context, BZCT seems to be a very promising material due to its exceptional ferroelectric properties [9]. Therefore, researchers are making continuous efforts to transfer the same performance from bulk ceramics to thin films as thin films are essential for miniaturizing electronic devices. Moreover, the energy storage performance of thin films is

* Corresponding author. Centre of Physics of University of Minho and Porto (CF-UM-UP), Campus de Gualtar, 4710-057, Braga, Portugal.
** Corresponding author.
E-mail addresses: josesilva@fisica.uminho.pt (J.P.B. Silva), kamakshik@iiitt.ac.in (K. Kamakshi).
[1] Equal contribution.

https://doi.org/10.1016/j.ceramint.2023.03.207
Received 26 January 2023; Received in revised form 9 March 2023; Accepted 21 March 2023
Available online 22 March 2023

usually higher than that of bulk ceramics due to the large electric breakdown field and maximum polarization achieved which makes the films more promising [10]. For instance, BZCT epitaxial films grown on $La_{0.67}Sr_{0.33}MnO_3$ (LSMO)-coated (100)-oriented MgO single crystal substrates exhibit a high discharge curve energy density ~27.5 J/cm^3 at a maximum electric field of 2.77 MV/cm [11]. Moreover, a high recoverable energy density value of 78.7 J/cm^3 and efficiency of 80.5%, at 6600 kV/cm, are achieved in $BaZr_{0.35}Ti_{0.65}O_3$ films grown by a radio-frequency sputtering technology on Nb:$SrTiO_3$ substrates [12]. However, the expensive price of single crystal substrates (e.g. Nb-doped $SrTiO_3$) limits their practical applications. Therefore, there is a need of depositing these materials on Si-based substrates. For instance, Reddy et al. reported on the polycrystalline BZCT films grown by sol-gel spin-coating on $Si/SiO_2/TiO_2/Pt(100)$ substrates. By optimizing the growth conditions, BZCT films can exhibit an energy storage density (ESD) of 64.8 J/cm^3 and an efficiency of 73% at 2000 kV/cm electric field [13]. Moreover, BZCT films exhibit an ESD of 9.5 J/cm^3, and this value drops to 2.7 J/cm^3 as the top electrode area increases from ~0.025 mm^2 to ~0.785 mm^2, due to sharp decrease in operational electric field [14]. Yet, the investigations reported in the literature to enhance the energy storage (ES) performance were not focused much on the effect of high electric field strength. The main task associated with a high electric field is the dielectric breakdown [15,16] and so another disadvantage focused on is the requirement of special shielding and insulating materials for the safeguard of the device components [17–19]. In this perspective, developing materials with high ES performance at a relatively lower electric field is the need of the hour for practical applications. Therefore, in the present work, we investigate the ES performance of BZCT-based films under a low electric field.

Therefore, we have chosen a complex BZCT-STO mixture $0.85[0.6Ba(Zr_{0.2}Ti_{0.8})O_3\text{-}0.4(Ba_{0.7}Ca_{0.3})TiO_3]\text{-}0.15SrTiO_3$ as it was recently shown that the incorporation of the paraelectric $SrTiO_3$ is a promising strategy to enhance the ES performance of the BZCT [3] for the fabrication of films. The effects of thickness on the microstructure, ferroelectric, resistive switching, and energy properties of BZCT-STO films deposited by pulsed laser deposition (PLD) are discussed and also highlighted underlying mechanisms. The BZCT-STO films with a thickness of 160 nm, prepared with an electrode area of 0.5 mm^2 exhibited good energy storage properties with ESD of 6.0 J/cm^3 with an efficiency of 72% at a field of 800 kV/cm, that is better than in Ref. [14] by taken into account of capacitor area and operational field due to relaxor type ferroelectric induced by smaller grain size, low c/a ratio, low k dielectric interfacial layer and high back switching ratio.

2. Experimental techniques

The $0.85[0.6Ba(Zr_{0.2}Ti_{0.8})O_3\text{–}0.4(Ba_{0.7}Ca_{0.3})TiO_3]\text{–}0.15SrTiO_3$ [BZCT–STO] ceramic targets were prepared using the conventional solid state reaction method and the detailed procedure is described in our previous work [3]. The BZCT-STO films were deposited on Pt/Ti/-SiO_2/Si substrate using the pulsed laser deposition with KrF laser of wavelength 248 nm, the energy density of 350 J and laser repetition rate of 2 Hz. The distance between the target and substrate is 70 mm. Before the deposition, the chamber is evacuated to a pressure of 2×10^{-6} mbar. The films were grown in the presence of O_2 atmosphere with 0.05 mbar pressure at a temperature of 750 °C and then annealed at 775 °C under 0.1 mbar O_2 atmosphere. We have grown BZCT-STO films under similar conditions, but with different thicknesses of 160 nm, 260 nm, and 360 nm.

The crystal structure of BZCT-STO films were scanned using an X-ray diffractor (Bruker D8 Discover) with a CuK_α wavelength of 0.154 nm. The surface morphology and cross-section of BZCT-STO films were recorded using field emission scanning electron microscopy (FEI NOVA model). To study the electrical properties top gold circular electrodes with an area of 0.5 mm^2 were deposited on the top surface of BZCT-STO films using the thermal evaporation technique. The current-voltage (I–V) characteristics of Pt/BZCT-STO/Au capacitors were investigated using a Keithley electrometer by applying bias from -5 V to +5 V in forward cycle and vice-versa in the reverse cycle. The ferroelectric properties of capacitors were investigated using a modified Sawyer-Tower circuit in metal-insulator-metal (MIM) configuration at different frequencies and different electric fields.

3. Results and discussion

3.1. Structure/microstructure studies

X-ray diffraction (XRD) patterns of the BZCT-STO target and corresponding films deposited on the $Pt/Ti/SiO_2/Si$ with different thicknesses are shown in Fig. 1. The (hkl) values of all the crystallographic reflection planes were indexed with JCPDS file number 05–0626, 85–0368 [3,29]. All the peaks corresponding to the tetragonal phase of bulk ceramics were observed in the films. Thus, the films show a polycrystalline perovskite phase without any secondary or impurity phases. However, the x-ray reflections in the films slightly shifted towards lower 2θ compared to a bulk position. The extended XRD scans around 2θ ~31.5° are shown in Fig. 1(b). It is possible to observe that the (110) peak for the BZCT-STO films is shifted towards lower 2θ when compared to the position of the same peak in the target and this shift is found to be increased with the decrease of thickness. This shift causes a change in lattice parameters. Therefore, lattice constants of the tetragonal structure were evaluated using equation (1), and the calculated lattice parameters "a" and "c" of the BZCT-STO target and the films are listed in Table 1 [20].

$$d_{\text{Tetragonal}} = \frac{1}{\sqrt{\frac{h^2+k^2}{a^2} + \frac{l^2}{c^2}}} \quad (1)$$

The lattice parameters were estimated by using most commonly used least square method [21]. In our previous work, we observe that the parameters estimated from this method is in good agreement with values estimated by TEM/SAED measurements in BTO films [22]. The lattice mismatch of bottom electrode (Pt is 0.392 nm) and films is generally adjusted in the form of strain in thin films. Further, the difference in thermal expansion coefficients of the film and the substrate also contribute to strain. The lattice parameters tend to approach to bulk as the film thickness increases and this suggests the weakening of substrate clamping effect and/or the relaxation of stain at higher thickness. Similar trend is observed in thickness dependent $(Ba_{0.5}Sr_{0.5})_{0.925}K_{0.075}TiO_3$ thin films and strain is relaxed when thickness is greater than 200 nm [23]. Further, it is observed that the tetragonality (c/a ratio) increases with the film thickness and a higher value of tetragonality (≈1.008) was found for the film with thickness of 360 nm. This value is slightly lower than the value estimated for the target (c/a = 1.009) [3].

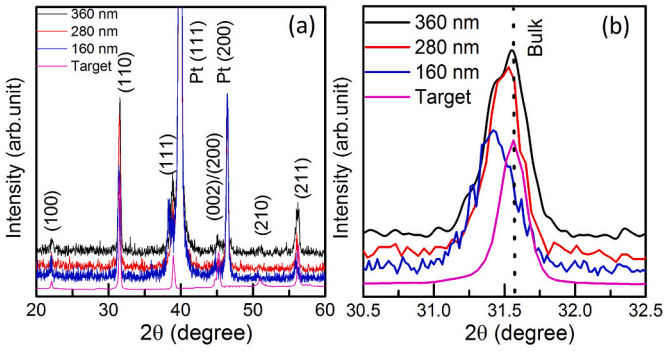

Fig:1. (a) XRD patterns of BZCT-STO target and corresponding films with different thickness and (b) Extended XRD scans around 2θ = 31.5°.

Table 1
Values of lattice parameters 'a' and 'c' and tetragonality ratio (c/a) for the films and the target.

Thickness of BZCT-STO films (nm)	a (Å)	c (Å)	Tetragonality ratio (c/a)
160	4.0182	4.0302	1.003
280	4.0087	4.0327	1.006
360	4.0072	4.0392	1.008
Bulk ceramic	4.0066	4.0429	1.009

The surface morphology of BZCT-STO thin films with thickness of 160 nm and 360 nm is depicted in Fig. 2(a) −2(b) respectively. The grain size distribution is given as inset in each micrograph. The average grain size was found to increase from 34 nm to 60 nm with the increase of thickness from 160 nm to 360 nm. The increase in grain size with increase of film thickness can be attributed to relaxation of strain in thicker films as evidenced from XRD analysis. Further, the film with thickness of 160 nm consists of uniform triangle shaped grains, whereas, the films with thickness of 260 and 360 nm consists of nearly spherical shape grains. The change in morphology at low thickness could be attribute to substrate effect. The cross-sectional image of the films is also shown in inset of the SEM micrograph; it confirms the thickness of Pt and BZCT films (160 and 360 nm). The energy dispersive x-ray spectrum (EDS) of BZCT-STO film with thickness of 160 nm as shown in Fig. 2(c), exhibited the characteristic peaks corresponding to the elements (Ba, Ti, Zr, Ca, Sr and O) of BZCT-STO films and elements (Pt, Ti, O and Si) corresponding to substrate. The absence of any other element in EDS is in good agreement with the absence of any secondary/impurity phase in the BZCT layer from XRD analysis.

3.2. Resistive switching properties

The current-voltage (I–V) characteristics of BZCT-STO films with thicknesses of 160 nm, 260 nm, and 360 nm were shown in Fig. 3(a)-(c) respectively. The absolute value of current at a bias voltage of -5 V is found to be decreased from 160 μA to 0.66 nA as the thickness increased from 160 to 360 nm. This suggests that the film at higher thickness becomes more insulating. The presence of large strain in low thickness films can cause higher leakage currents in ferroelectric thin films [23]. Many factors like grain size, grain boundaries, misfit strain, misfit dislocations, and dielectric interface layer at film-electrode interface can effect overall leakage currents in films. Another important parameter that effect leakage current in ferroelectric thin films is depolarization field. Here, we assumed that the thickness and dielectric constant of dielectric interface layer (d) is same in all films as all experimental conditions are same [23]. However, the ratio of d/L (Where L is thickness of ferroelectric layer) is crucial as depolarization field decreases with decrease of d/L and thus, interfacial dielectric layer is significant at low thickness [24]. The depolarization field can form the depletion region at the interface similar to Schottky diode and causes the rectification behavior. The rectifying ratio i.e ratio of current at -5 V and +5 V (I_{-5V}/I_{5V}) is found to be 293, 2.1, and 1.4 for the films with thickness of 160, 260, and 360 nm respectively. The high rectifying ratio in the film at 160 nm can be attributed to Schottky barrier and the substrate clamping effect [25,26]. The non-rectifying behavior in film with thickness of 360 nm evidences same that strong ferroelectric polarization vanishes the depletion region due to negligible depolarization field.

More interestingly, the I–V characteristics of BZCT-STO thin films exhibited a resistive switching (RS) effect. The resistive switching ratios i.e ratios of low resistance state (LRS) and high resistance state (HRS), at a voltage of +3 V for the films with thicknesses of 160 and 260 nm are found to be 280 and 145 respectively. Whereas, RS ratio is found to be 97 at +1 V for the film with a thickness of 360 nm. The RS effect in the ferroelectric capacitors is due to the modulation of the Schottky barrier by intrinsic ferroelectric polarization [26]. Usually, the Schottky barrier is formed due to the different work functions of the top and bottom electrodes (5.65 eV for Pt and for 4.74 eV for Au). Further, formation of Schottky barrier at metal-film interface is very complex phenomenon as dependent on many factors like grain size, grain boundaries and screening length besides electrode's work function and the ferroelectric's electron affinity. It is commonly accepted that the charge carriers are trapped at localized defects in grain boundaries/misfit dislocations and creates space charge region and enhances potential barrier [27,28]. Further, the depolarization in ferroelectrics contribute to Schottky barrier due to incomplete compensation of charge carriers [29]. Moreover, the Schottky barrier is lowered ($\varnothing_B^{'}$) by polarization as follows

$$\varnothing_B^{'} = \varnothing_B - \sqrt{\frac{qP}{4\pi\varepsilon_d\varepsilon_s\varepsilon_o^2}} \quad (2)$$

Where $\varnothing_B$ is Schottky barrier at zero potential and ε_s and ε_d are static (low frequency) and dynamic (high frequency) dielectric permittivity of ferroelectric material [30]. Thus, the Schottky barrier lowering ($\varnothing_B^{'}$) is different for different thickness and thus shows the effect on leakage currents accordingly. Since ferroelectric polarization enhanced with the increase in thickness of BZCT-STO films, one should expect Schottky barrier is lowered and thus causes low switching in higher thick films. Moreover, the d/L ratio is significant at low thickness and causes high

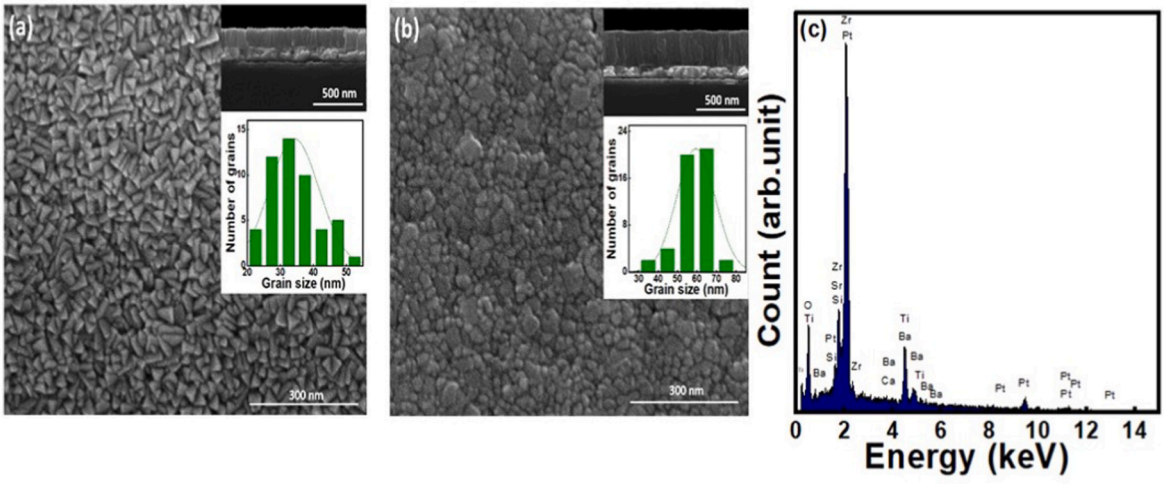

Fig. 2. Surface morphology of the BZCT-STO films deposited with a thickness of (a) 160 nm (b) 360 nm. Insets showing their corresponding cross-sectional images and grain size distributions are included (c) EDS spectrum of BZCT-STO film with thickness of 160 nm.

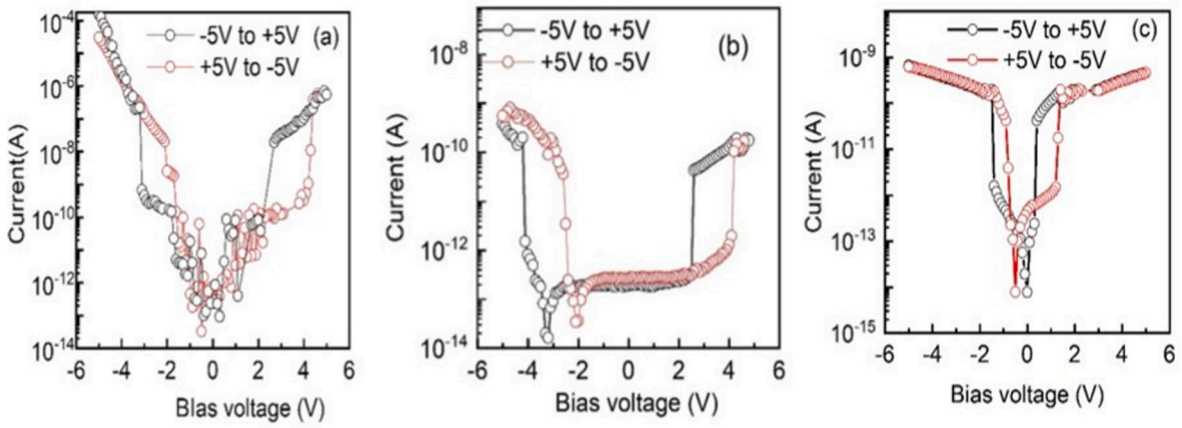

Fig. 3. Current-voltage characteristics of Pt/BZCT-STO/Au capacitors with BZCT-STO thickness of (a) 160 nm, (b) 260 nm and, (c) 360 nm.

switching ratio. This is in good agreement with our previous work, where the insertion of a thin dielectric layer between the electrode and film enhances the RS effect in a ferroelectric-dielectric heterostructures [22]. The switching voltage for the film with a thickness of 360 nm is low compared to films with a thickness of 260 and 160 nm. This also supports the effect of an interfacial dielectric layer. One can assume that a thin dielectric layer is in series with a ferroelectric layer and the most of the applied field is dropped across this dielectric layer. This makes the necessity of high field for polarization reversal. Under the –Ve to +Ve sweep direction, the capacitor is in high resistance state (HRS) due to the depletion of charges at the passive dielectric–ferroelectric interface until the positive voltage reaches to coercive field. Beyond this field, due to polarization reversal, a charge accumulation occurs at the dielectric-film interface and thus, the Schottky barrier becomes lower. Consequently, the capacitor reaches the LRS state.

3.3. Ferroelectric properties

The ferroelectric properties of Pt/BZCT-STO/Au capacitors with different thicknesses were studied at an electric field up to 250 kV/cm and are shown in Fig. 4(a). The hysteresis behaviour of P-E loops confirms the ferroelectric nature of films, which is strongly dependent on the thickness of the film. Further, the butterfly features of polarization current versus a.c. electric field as shown in Fig. 4 (b) for the film with thickness of 260 nm corroborate the ferroelectric nature of BZCT-STO films. When the field is swept from −250 kV/cm to +250 kV/cm, the

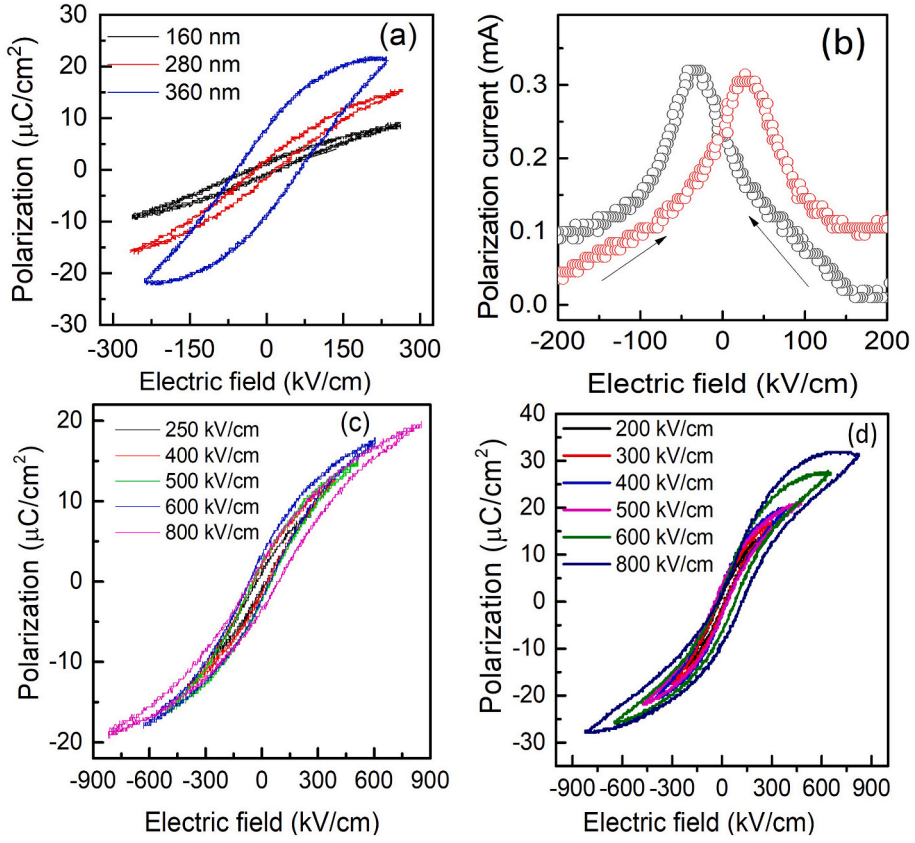

Fig. 4. (a) P-E hysteresis loops of Pt/BZCT-STO/Au capacitors with different thicknesses, up to 250 kV/cm. (b) Plot of polarization current versus electric field of BZCT-STO film with a thickness of 260 nm (c)–(d) Field dependent P-E loops of BZCT-STO films with a thickness of 160 and 260 nm.

current maxima occurs on positive field side and vice-versa for the field swept from +250 kV/cm to −250 kV/cm. This is due to the domain switching of polarization from one direction to other direction [31]. The gradual increase in polarization current with field is due to nucleation and growth of domains in the field direction. The field corresponding to the peak in current density can be considered coercive field at which most of the domain reversal occurs. Beyond the peak, the decrease in polarization current is due to saturation of polarization/reduction in mobility of domain walls due to coalescence. Thus, P-E and I-E evolutions confirm the ferroelectric nature of films. The variation of remnant polarization (P_r), the maximum polarization (P_m) and the coercive field (E_c) is shown in Table 2. The values of P_r and P_m are found to be increasing with the increase of the BZCT-STO thickness. Various factors like interface layer, leakage currents, and substrate clamping effect are to be considered. From I–V and P-E studies, one can observe that the influence of leakage current on the ferroelectric polarization decreased as the thickness of the film increased. The increase in polarization with an increase in thickness can be attributed to the weak effect of substrate clamping, interface layer, and high tetragonality ratio evidenced by XRD analysis. The field dependent P-E hysteresis loops for films with a thickness of 160 nm and 260 nm were studied as shown in Fig. 4(c) and 4 (d) respectively. It is obvious that polarization values are increased with the increase of field due to the contribution of new domains in addition to existing domains [32]. It is noticed that P-E loops become more lossy beyond 800 kV/cm for thinner film (not shown here) could be due to dielectric break down.

The films with lower thickness (160 nm and 260 nm) exhibited relaxor-type ferroelectric. It has been reported that a slim and slant hysteresis loop is typical of relaxor ferroelectrics nature [33]. At low thicknesses, the depolarization field (E_{de}) plays a crucial role in shaping the P-E loops. Usually, the E_{de} can be expressed as follows [34].

$$E_{de} = \frac{P_f d}{\varepsilon_0 \left(\varepsilon_d l + \varepsilon_f d\right)} \tag{3}$$

Where P_f is the ferroelectric polarization, l is the ferroelectric film thickness, d is the thickness of the interface layer, and ε_0, ε_f and ε_d are the permittivity of free space, the ferroelectric layer, and the interface layer respectively. If we assume that interface layer characteristics, like thickness and dielectric constant, are the same for all the films, from the above equation (3) it is evident that the E_{de} becomes higher with the decreasing thickness of the ferroelectric layer and thus the hysteresis loops become slimmer. Further, the origin of relaxor behavior can also be attributed to the grain size effect. The larger grain size in the films with a thickness of 360 nm as evidenced from SEM analysis suggested that a larger gain size is beneficial to achieve higher P_r, as the repulsion force among adjacent domain walls decreases and thus enhances domain wall flexibility. Usually, both 180° and non-180° domain walls contribute to the polarization reversal. The relative contribution of 180° and non-180° can be estimated by using back switching ratio which is defined as follows [35].

$$\textit{Back switching} \text{ ratio } (\%) = \left(1 - \frac{P_r}{P_s}\right) \times 100 \tag{4}$$

The back switching ratio is found to be minimum for the film thickness of 360 nm and suggests that it has relatively more 180° domains due to the larger grain size. The low grain size favours polar nano regions (PNRs), which is identified as the primary reason for the existence of relaxor behavior. Moreover, a reduction in the tetragonality ratio with the decrease of film thickness also supports relaxor-type ferroelectric at a low thickness. The relaxor ferroelectric materials are more attractive for energy storage application due to their low hysteresis loss as compared to normal ferroelectrics [33].

Table 2
The effect of thickness on Pr, Ps, E_c and back-switching ratio of BZCT-STO films.

Thickness of film (nm)	P_r (μC/cm^2)	P_m (μC/cm^2))	E_c (kV/cm)	Back switching ratio (%)
160	1.3	8.3	21.5	85
260	1.9	14.9	16.2	87
360	8.1	21.9	62.2	63

3.4. Energy storage performance

The energy storage properties of BZCT-STO thin films were evaluated using a P-E loop as shown in Fig. 5(a). The recoverable energy density (W_r) and efficiency are calculated as follows [33].

$$W_r = \int_{P_r}^{P_m} EdP \tag{5}$$

and

$$\eta = \left(\frac{W_r}{W_r + W_l}\right) \tag{6}$$

Where W_l is energy loss due to hysteresis/area of P-E loop.

The estimated values of W_r, W_l, and η for BZCT-STO films with different thicknesses are shown in Fig. 5(b). The recoverable energy density is increased from 0.7 to 1.3 J/cm^3 as the thickness increases from 160 to 260 nm and then decreased to 1 J/cm^3 with a further increase of thickness to 360 nm. This is due to the sharp increase of P_r at higher thicknesses. Further, the efficiency of capacitors with thicknesses of 160 and 260 nm is found to be 73% and 72%, whereas the capacitor with a thickness of 360 nm exhibited a very low efficiency (31%) due to high hysteresis loss. The sharp decrease in W_r and η in the film with a thickness of 360 nm can be understood as follows: According to modified LGC theory the spontaneous polarization (P_s) can relate to grain size (G) and tetragonality ratio (c/a) as follows [36].

$$P_s^2 \propto G \propto \frac{c}{a} \tag{7}$$

From XRD and SEM analysis, we observe that G and c/a ratio is maximum and thus P_s is higher as evident from P-E loops at thickness of 360 nm. Further, the larger grain size facilitates formation multi-domains as the domain size is proportional to square of grain size and strengthen long-range ferroelectric order. In this case, high P_r is expected and consequently, larger hysteresis width [37]. The high P_r and large hysteresis width decreases W_r and η. Therefore, the high recoverable energy density and efficiency of films at low thickness are attributed to small grain size, lower tetragonality, and high back-switching ratio. Thus, we have chosen the BZCT-STO films with a thickness of 160 nm and 260 nm for further investigation of energy storage properties.

The effect of the electric field on the energy storage properties of BZCT-STO thin films was evaluated in an electric field range of 250 kV/cm to 1000 kV/cm. The W_r, and η values as a function of the electric field for films the thickness of 160 and 260 nm are shown in Fig. 5(c). It is worth observing that in both cases, W_r increases sharply with the field based on the fact that polarization is a field-dependent parameter. However, the film with a thickness of 160 nm shows an efficiency $\geq$ 72% whereas the efficiency sharply declined with the field in the case of the film with a thickness of 260 nm. This may be due to the existence of more PNRs in the thinnest film due to the low grain size [37]. The present film shows more than 2.5 times of ESD as compared to BCZT film deposited on single crystal substrate with similar area of electrodes [14]. Further, Pt–Si substrates are cheaper and more compatible for practical applications compared to single crystal substrates. The energy-storage coefficient (W_r/E) is an important parameter to evaluate the energy storage performance of the capacitors [39]. The energy-storage coefficient was found to be 0.0071 JkV^{-1}cm^{-2} and 0.0081 JkV^{-1}cm^{-2} for the films with the thickness of 160 and 260 nm respectively. This value is comparable to the one observed in the literature for NBT and BT-based

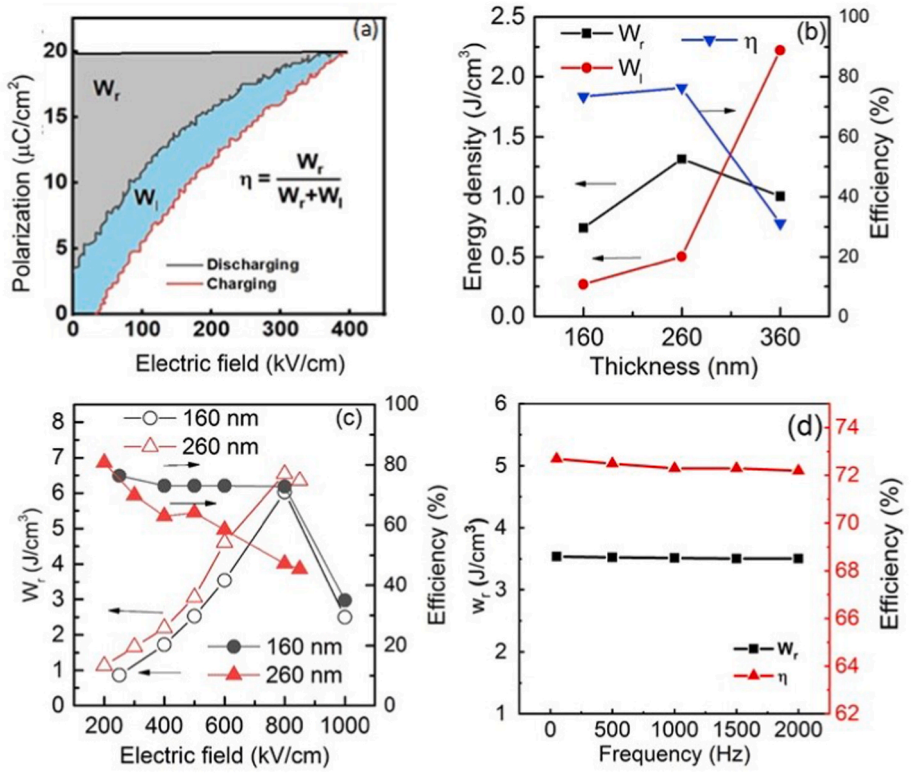

Fig. 5. (a) schematic representation of energy storage parameters for BZCT-STO film with a thickness of 260 nm (b): the variation of W_r, W_l and η as a function of thickness; (c) the variation of W_r, and η as a function of electric field and (d): the variation of W_r, and η as a function of frequency for BZCT-STO films with a thickness of 160 nm at a field of 600 kV/cm.

film capacitors [38].

Further, the effect of frequency on the energy storage properties of BZCT-STO thin films with thickness of 160 nm was evaluated at an electric field of 600 kV/cm. The frequency-dependent W_r and η is shown in Fig. 5 (d). The robust nature of W_r and η with a frequency suggested the contribution to the polarization is dominated by dipole orientations rather than space charges and/or defects. Thus, Pt/BZCT-STO/Au capacitors are stable for an operation at a wide range of frequencies. Furthermore, Fig. 6 shows the effect of the number of charging/discharging cycles on the recoverable energy density of the film with a thickness of 160 nm. There is no significant change in the energy storage parameters both recoverable energy density and efficiency up to 10^8 cycles. Thus, the robust energy storage performance of BZCT-STO film with a thickness of 160 nm makes it attractive for energy storage capacitor applications.

4. Conclusions

In this work, the effect of the thickness of BZCT-STO on its microstructure, resistive switching, ferroelectric and energy storage properties of Pt/BZCT-STO/Au capacitors were investigated in detail. The XRD analysis suggest BZCT-STO films were polycrystalline with tetragonal structure and the strain was relaxed according to the increase of thickness. SEM analysis revealed dense columnar structure with different shape and grain size depending also on the thickness of the film. The ferroelectric and electric properties were strongly influenced by interfacial low k dielectric layer formed at Pt-BZCT interface in thin films. The PT/BZCT-STO/Au capacitor with thickness of 160 nm exhibited optimum switching ratio of 260 due to prominent effect of interfacial layer. The slim and slant P-E loops in thinner films were attributed to small grain size, interfacial layer, high depolarization and PNRs, which are beneficial for energy storage applications. The effect of thickness, electric field and frequency on the energy storage properties of BZCT-STO films investigated. The BZCT-STO film with thickness of 160 nm exhibited superior energy storage properties with W_r of 6.0 J/cm^3 and an efficiency of 72% at a field of 800 kV/cm. The energy storage performance was robust in the frequency range of 50–2000 Hz and up to 10^8 cycles passing through the device.

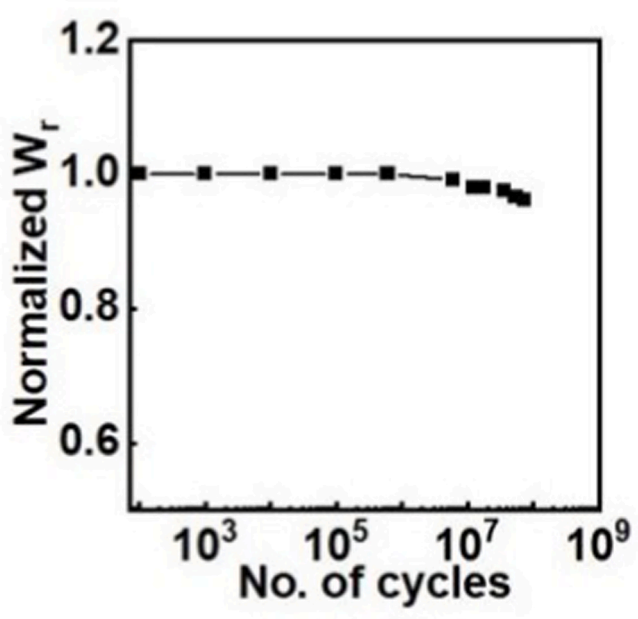

Fig. 6. Effect of number of cycles on energy density of BZCT-STO film with a thickness of 160 nm.

Declaration of competing interest

The authors declare that they have no known competing financial interests or personal relationships that could have appeared to influence the work reported in this paper.

Acknowledgment

This work was supported by the Portuguese Foundation for Science and Technology (FCT) in the framework of the Strategic Funding Contract UIDB/04650/2020. This work has received funding from the European Union's Horizon 2020 research and innovation program under grant agreement No 958174 (M-ERA-NET3/0003/2021—NanOx4EStor). The author KK acknowledges DST –SERB for the financial support through grant no: SPG/2021/003797. The authors would also like to thank José Santos for technical support in the Thin Film Laboratory at CF-UM-UP.

References

[1] J.F. Scott, C.A. Paz de Araujo, Ferroelectric memories, Sci (New York, N.Y.). 246 (1989) 1400–1405, https://doi.org/10.1126/science.246.4936.1400.

[2] V.S. Puli, D.K. Pradhan, S. Adireddy, R.V. Martínez, P. Silwal, J.F. Scott, V. R. Chintalpalli, D.B. Chrisey, R.S. Katiyar, Observation of large enhancement in energy-storage properties of lead-free polycrystalline $0.5BaZr_{0.2}Ti_{0.8}O_3$–$0.5Ba_{0.7}Ca_{0.3}TiO_3$ ferroelectric thin films, J. Phys. D Appl. Phys. 48 (2015), 355502, https://doi.org/10.1088/1361-6463/ab161a.

[3] A.R. Jayakrishnan, K.V. Alex, K. Kamakshi, J.P.B. Silva, K.C. Sekhar, M.J. M. Gomes, Semiconductor/relaxor 0-3 type composites: a novel strategy for energy storage capacitors, Enhancing the dielectric relaxor behavior and energy storage properties of $0.6Ba(Zr_{0.2}Ti_{0.8})O_3$–$0.4(Ba_{0.7}Ca_{0.3})TiO_3$ ceramics through the incorporation of paraelectric $SrTiO_3$, J. Mater. Sci. Mater. Electron. 30 (21) (2019) 19374–19382, https://doi.org/10.1016/j.jsamd.2020.09.012.

[4] S. Chen, X. Wang, T. Yang, J. Wang, Enhanced energy storage properties and temperature stability of fatigue-free La-modified $PbZrO_3$ films under low electric fields, J. Electroceram. 32 (2014) 307–310, https://doi.org/10.1007/s10832-014-9900-x.

[5] X. Hao, Y. Wang, J. Yang, S. An, J. Xu, High energy-storage performance in $Pb_{0.91}La_{0.09}$ $(Ti_{0.65}Zr_{0.35})$ O_3 relaxor ferroelectric thin films, J. Appl. Phys. 112 (11) (2012), 114111, https://doi.org/10.1063/1.4768461.

[6] Q. Zhang, Y. Dan, J. Chen, Y. Lu, T. Yang, X. Yao, Y. He, Effects of composition and temperature on energy storage properties of $(Pb,La)(Zr,Sn,Ti)O_3$ antiferroelectric ceramics, Ceram. Int. 43 (2017) 11428–11432, https://doi.org/10.1016/j.ceramint.2017.06.005.

[7] Q. Zhang, X. Liu, Y. Zhang, X. Song, J. Zhu, I. Baturin, J. Chen, Effect of barium content on dielectric and energy storage properties of $(Pb,La,Ba)(Zr,Sn,Ti)O_3$ ceramics, Ceram. Int. 41 (2015) 3030–3035, https://doi.org/10.1016/j.ceramint.2014.10.139.

[8] I. Coondoo, N. Panwar, A. Kholkin, Lead-free piezoelectrics: current status and perspectives, J. Adv. Dielectric. 3 (2013), 1330002, https://doi.org/10.1142/S2010135X13300028.

[9] J.P.B. Silva, J.M.B. Silva, M.J.S. Oliveira, T. Weingärtner, K.C. Sekhar, M. Pereira, M.J.M. Gomes, High-performance ferroelectric–dielectric multilayered thin films for energy storage capacitors, Adv. Funct. Mater. 29 (2019), 1807196, https://doi.org/10.1002/adfm.201807196.

[10] A.R. Jayakrishnan, J.P.B. Silva, K. Kamakshi, D. Dastan, V. Annapureddy, M. Pereira, K.C. Sekhar, Are lead-free relaxor ferroelectric materials the most promising candidates for energy storage capacitors? Prog. Mater. Sci. 132 (2023), 101046 https://doi.org/10.1016/j.pmatsci.2022.101046.

[11] V.S. Puli, D.K. Pradhan, K. Madgula, S.N. Babu, M. Laad, D.B. Chrisey, R.S. Katiyar, A. Reed, T. Back, M.E. Mc Conney, R.M. Van Ginhoven, S. Heidger, Enhanced energy storage properties of epitaxial $(Ba_{0.955}Ca_{0.045})(Zr_{0.17}Ti_{0.83})O_3$ ferroelectric thin films, Energy Storage 4 (2022), e330, https://doi.org/10.1002/est2.330.

[12] Z. Liang, M. Liu, C. Ma, L. Shen, L. L, Chun-Lin Jia, High-performance $BaZr_{0.35}Ti_{0.65}O_3$ thin film capacitors with ultrahigh energy storage density and excellent thermal stability, J. Mater. Chem. A. 6 (2018) 12291–12297, https://doi.org/10.1039/C7TA11109F.

[13] S.R. Reddy, V.V.B. Prasad, S. Bysakh, V. Shanker, N. Hebalkar, S.K. Roy, Superior energy storage performance and fatigue resistance in ferroelectric BCZT thin films grown in an oxygen-rich atmosphere, J. Mater. Chem. C 7 (2019) 7073–7082, https://doi.org/10.1039/C9TC00569B.

[14] S. He, B. Peng, G.J.T. Leighton, C. Shaw, N. Wang, W. Sun, L. Liu, Q. Zhang, High-performance La-doped BCZT thin film capacitors on LaNiO3/Pt composite bottom electrodes with ultra-high efficiency and high thermal stability, Ceram. Int. 45 (2019) 11749–11755, https://doi.org/10.1016/j.ceramint.2019.03.051.

[15] A. Chauhan, S. Patel, R. Vaish, C.R. Bowen, Anti-ferroelectric ceramics for high energy density capacitors, Materials 8 (12) (2015) 8009–8031, https://doi.org/10.3390/ma8125439.

[16] W.V. Hassenzahl, D.W. Hazelton, B.K. Johnson, P. Komarek, M. Noe, C.T. Reis, Electric power applications of superconductivity, Proc. IEEE 92 (2004) 1655–1674, https://doi.org/10.1109/JPROC.2004.833674.

[17] J. Gao, Y. Wang, Y. Liu, X. Hu, X. Ke, L. Zhong, Y. He, X. Ren, Enhancing dielectric permittivity for energy-storage devices through tricritical phenomenon, Sci. Rep. 7 (2017), 40916, https://doi.org/10.1038/srep40916.

[18] M. Hara, J. Gerhold, Electrical insulation specification and design method for superconducting power equipment, Cryogenics 38 (11) (1998) 1053–1061, https://doi.org/10.1016/S0011-2275(98)00093-9.

[19] S.R. Reddy, V.V.B. Prasad, S. Bysakh, V. Shanker, N. Hebalkar, S.K. Roy, Superior energy storage performance and fatigue resistance in ferroelectric BCZT thin films grown in an oxygen-rich atmosphere, J. Mater. Chem. C 7 (2019) 7073–7082, https://doi.org/10.1039/C9TC00569B.

[20] L.J. Sinnamon, M.M. Saad, R.M. Bowman, J.M. Gregg, Exploring grain size as a cause for "dead-layer" effects in thin film capacitors, Appl. Phys. Lett. 81 (2002) 703, https://doi.org/10.1063/1.1494837.

[21] M.J.S. Oliveira, J.P.B. Silva, K. Veltruská, V. Matolín, K.C. Sekhar, J. Agostinho Moreira, M. Pereira, M.J.M. Gomes, Annealing induced effect on the physical properties of ion-beam sputtered $0.5Ba(Zr_{0.2}Ti_{0.8})O_3$–$0.5(Ba_{0.7}Ca_{0.3})TiO_{3-\delta}$ ferroelectric thin films, Appl. Surf. Sci. 443 (2018) 354–360, https://doi.org/10.1016/j.apsusc.2018.02.269.

[22] J.P.B. Silva, F.L. Faita, K. Kamakshi, K.C. Sekhar, J.A. Moreira, A. Almeida, M. Pereira, A.A. Pasa, M.J.M. Gomes, Enhanced resistive switching characteristics in Pt/$BaTiO_3$/ITO structures through insertion of HfO_2:Al_2O_3 (HAO) dielectric thin layer, Sci. Rep. 7 (2017), 46350, https://doi.org/10.1038/srep46350.

[23] K.C. Sekhar, S.H. Key, K.P. Hong, C.S. Han, J.M. Yook, D.S. Kim, J.C. Kim, J. Chul Park, Y.S. Cho, Thickness-dependent tunable characteristics of $(Ba_{0.5}Sr_{0.5})$ $_{0.925}$ $K_{0.075}TiO_3$ thin films prepared by pulsed laser deposition, Curr. Appl. Phys. 12 (2012) 654–658, https://doi.org/10.1016/j.cap.2011.09.017.

[24] J.M.B. Silva, J.P.B. Silva, K.C. Sekhar, M. Pereira, M.J.M. Gomes, Impact of the ferroelectric layer thickness on the resistive switching characteristics of ferroelectric/dielectric structures, Appl. Phys. Lett. 113 (2018), 102904, https://doi.org/10.1063/1.5047853.

[25] J.P.B. Silva, K.C. Sekhar, S.A.S. Rodrigues, M. Pereira, A. Parisini, E. Alves, N. P. Barradas, M.J.M. Gomes, On the formation of an interface amorphous layer in nanostructured ferroelectric $Ba_{0.8}Sr_{0.2}TiO_3$ thin films integrated on Pt–Si and its effect on the electrical properties, Appl. Surf. Sci. 278 (2013) 136–141, https://doi.org/10.1016/j.apsusc.2012.11.161.

[26] K.C. Sekhar, J.P.B. Silva, K. Kamakshi, M. Pereira, M.J.M. Gomes, Semiconductor layer thickness impact on optical and resistive switching behavior of pulsed laser deposited $BaTiO_3$/ZnO heterostructures, Appl. Phys. Lett. 102 (2013), 212903, https://doi.org/10.1063/1.4809531.

[27] T. Prakash, S. Ramasamy, B.S. Murty, Effect of DC bias on electrical conductivity of nanocrystalline α-CuSCN, AIP Adv. 1 (2011), 022107, https://doi.org/10.1063/1.3583601.

[28] C.M. Wu, E.S. Yang, Modification of Schottky barrier height by surface grain boundaries of polycrystalline silicon, Appl. Phys. Lett. 37 (1980) 945–947, https://doi.org/10.1063/1.91770.

[29] J. Tian, Z. Tan, Z. Fan, D. Zheng, Y. Wang, Z. Chen, F. Sun, D. Chen, M. Qin, M. Zeng, X. Lu, X. Gao, J. Liu, Depolarization-field-induced retention loss in ferroelectric diodes, Phys. Rev. Appl. 11 (2019), 024058, https://doi.org/10.1103/PhysRevApplied.11.024058.

[30] L. Pintilie, I. Vrejoiu, D. Hesse, G. LeRhun, M. Alexe, Ferroelectric polarization-leakage current relation in high quality epitaxial Pb (Zr, Ti) O_3 films, Phys. Rev. B 75 (2007), 104103, https://doi.org/10.1103/PhysRevB.75.104103.

[31] K.C. Sekhar, Arvind Nautiyal, R. Nath, Structural and ferroelectric properties of spray deposited sodium nitrite:poly(vinyl alcohol) composite films, J. Appl. Phys. 105 (2009), 024109, https://doi.org/10.1063/1.3072626.

[32] K.C. Sekhar, R. Nath, Polarization reversal behavior of spray deposited sodium nitrite:poly(vinyl alcohol) composite films, Appl. Phys. Lett. 94 (2009), 102905, https://doi.org/10.1063/1.3098355.

[33] K. Shibata, F. Oka, A. Nomoto, T. Mishima, I. Kanno, Crystalline structure of highly piezoelectric (K,Na)NbO_3 films deposited by RF magnetron sputtering, Jpn. J. Appl. Phys. 47 (2008) 8909–8913, https://doi.org/10.1143/JJAP.47.8909.

[34] M. Mai, C. Zhu, G. Liu, X. Ma, Effect of dielectric layer on ferroelectric responses of P(VDF-TrFE) thin films, Phys. Lett. A. 382 (2018) 2372–2375, https://doi.org/10.1016/j.physleta.2018.05.049.

[35] M.H. Lente, A. Picinin, J.P. Rino, J.A. Eiras, 90° domain wall relaxation and frequency dependence of the coercive field in the ferroelectric switching process, J. Appl. Phys. 95 (2004) 2646, https://doi.org/10.1063/1.1645980.

[36] Zhe Zhao, V. Buscaglia, M. Viviani, M.T. Buscaglia, L. Mitoseriu, A. Testino, M. Nygren, M. Johnsson, Paolo Nanni, Grain-size effects on the ferroelectric behavior of dense nanocrystalline $BaTiO_3$ ceramics, Phys. Rev. B 70 (2004), 024107, https://doi.org/10.1103/PhysRevB.70.024107.

[37] C. Ziebert, H. Schmitt, J.K. Krüger, A. Sternberg, K.-H. Ehses, Grain-size-induced relaxor properties in nanocrystalline perovskite films, Phys. Rev. B 69 (2004), 214106, https://doi.org/10.1103/PhysRevB.69.214106.

[38] N. Sun, Y. Li, X. Liu, X. Hao, High energy-storage density under low electric field in lead-free relaxor ferroelectric film based on synergistic effect of multiple polar structures, J. Power Sources 448 (2020), 227457, https://doi.org/10.1016/j.jpowsour.2019.227457.